

Chapter 5

SYNTHESIS OF SITE-DIFFERENTIATED $[\text{Fe}_4(\mu_4\text{-O})]$ COMPLEXES
SUPPORTED BY PYRAZOLATE LIGANDS POSSESSING PENDANT
HYDROGEN BOND DONORS

Abstract

The synthesis of site-differentiated $[\text{Fe}_4(\mu_4\text{-O})]$ clusters supported by a hexa(pyridyl) tris(alkoxide)ligand and two different types of pyrazolates is described. Building off previous results with phenyl pyrazolate supporting ligands, sterically smaller scaffolds are explored using parent pyrazolate and 3-aminophenyl pyrazolate. The aminophenyl substituents were utilized to successfully construct a secondary coordination sphere hydrogen bonding network capable of forming stabilizing interactions with terminal chloride and hydroxide ligands bound to the apical Fe center. Terminal chloride and azide complexes were also synthesized with the parent pyrazolate ligand to directly compare spectroscopic parameters with the analogous complexes containing hydrogen bonding networks. Cyclic voltammetry experiments and Mössbauer spectroscopy were utilized to better understand the properties of the described clusters.

INTRODUCTION

The biological activation of many small molecules including dihydrogen, dioxygen, carbon dioxide, water, and dinitrogen is accomplished at complicated multimetallic active sites capable of managing the delivery of protons and electrons to and/or from the substrate.¹ The use of multiple metal centers to store oxidizing equivalents is exemplified by the [Mn₄Ca] cluster in the oxygen evolving complex (OEC) of photosystem II (PSII), which catalyzes the conversion of water into molecular oxygen.^{1h,2} The reverse reaction, dioxygen reduction to water, can be accomplished by cytochrome *c* oxidase as well as multicopper oxidases, such as laccase.^{1g,3} Beyond the careful control of cluster nuclearity and metal identity, Nature also frequently employs hydrogen bonding networks or acid/base moieties to help facilitate these chemical transformations.⁴ In P450 enzymes a complicated hydrogen bonding network helps to stabilize dioxygen binding and is also instrumental in mediating proton transfer.^{4a,5}

The use of secondary coordination sphere effects has become increasingly common in synthetic systems relevant to biological dioxygen reduction⁶ or water oxidation⁷ in recent years. In Fe complexes, terminal Fe(III)- and Fe(IV)-oxo as well as Fe(III)-sulfide and -selenide compounds derived from their elemental sources have been isolated utilizing tris(amido)amine scaffolds with stabilizing hydrogen bonding networks (Figure 2).⁸ More recently, nitrite reduction to nitric oxide and a terminal oxo moiety has also been recently observed in an azafulvene tripodal scaffold with Fe (Figure 2).⁹ These results demonstrate the ability of these types of scaffolds to fundamentally change the types of accessible Fe complexes by stabilizing reactive oxygenic species. While this strategy has been most commonly employed in monometallic systems, examples of dinuclear systems have also been reported.¹⁰

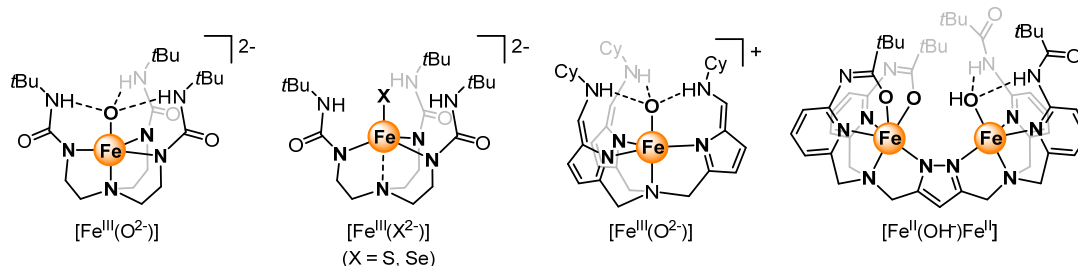


Figure 2. Literature examples of Fe and Cu complexes with pendant hydrogen-bonding moieties.

Our group has recently reported the synthesis of a series of tetrairon (μ_4 -oxido) ($[\text{Fe}_4(\mu_4\text{-O})]$) clusters (Figure 2).¹¹ Notably, these complexes showed four isolable oxidation states with localized redox behaviour isolated in the triiron core rather than the site-differentiated apical iron center based on solid-state structural analysis and Mössbauer data. While the apical Fe center is 4-coordinate as synthesized, the isolation of a series of complexes with nitric oxide (NO) coordinated to the apical iron center also proved accessible enabling the use of NO molecule as an IR reporter for the electronics of apical metal as a function of the triiron core oxidation state (Figure 2). Additional studies with oxygen atom transfer reagents with these clusters resulted in C–H or C–F bond activation and coordination of the resultant phenoxide to the apical iron center as shown in Figure 2. While no characterization of the reactive species is presently available these data suggest the ability oxygen atom transfer reagents to work in conjunction with $[\text{Fe}_4(\mu_4\text{-O})]$ core to accomplish the intramolecular activation of strong aryl-X bonds. Herein we report efforts to further elaborate the range of accessible $[\text{Fe}_4(\mu_4\text{-O})]$ -type clusters by further functionalizing the existing the pyrazolates scaffold to include hydrogen bonding moieties in an effort to stabilize reactive oxygenic species at the apical Fe. Efforts to open the steric congestion at the

apical Fe center to promote intermolecular reactivity and expand the variety of small molecules capable of binding were also pursued.

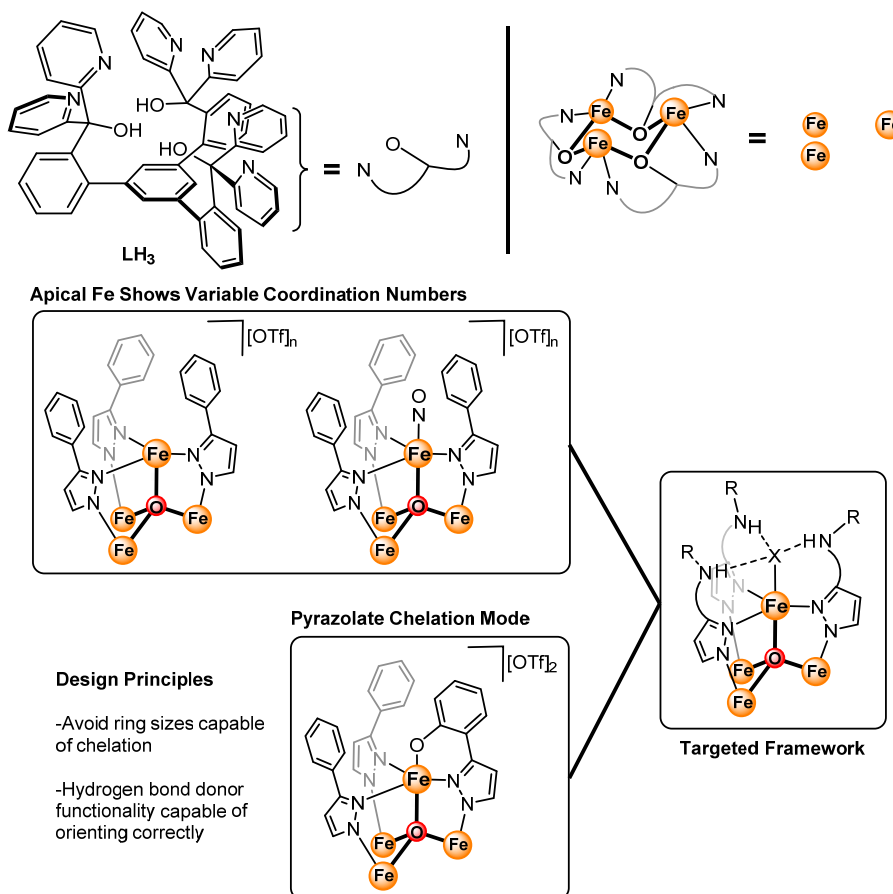


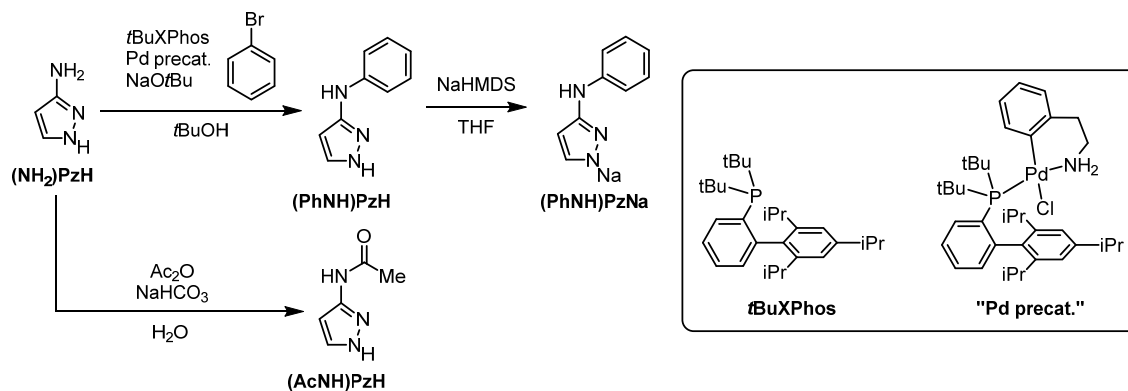
Figure 2. Outline of the design principles for the targeted ligand framework
RESULTS AND DISCUSSION

Section 5.1 Ligand Synthesis

The general synthetic strategy aimed to construct hydrogen bonding networks by modifying the established strategies employed for previously reported $[\text{Fe}_4(\mu_4\text{-O})]$ phenyl pyrazolate-supported clusters in our group. Starting from 3-amino pyrazole ($(\text{NH}_2)\text{PzH}$), multiple hydrogen bonding scaffolds were targeted (Scheme 1). $(\text{NH}_2)\text{PzH}$ is preceded to undergo Buchwald-Hartwig couplings with a variety of aryl and aromatic heterocyclic substrates to selectively afford mono-functionalized

product.¹² These conditions were utilized to afford 3-aminophenyl pyrazole ((**PhNH**)**PzH**) in multigram quantities. (**PhNH**)**PzH** could then be quantitatively deprotonated using sodium hexamethyldisilazide (NaHMDS) for afford the corresponding pyrazolate salt of the ligand ((**PhNH**)**PzNa**). The N-acetylation of (**NH₂**)**PzH** was accomplished according to a reported patent procedure to afford (**AcNH**)**PzH**, however, due to the initial successes observed with (**PhNH**)**PzNa** further efforts with this ligand were not pursued.

Scheme 1. Synthesis of hydrogen bonding pyrazole derivatives

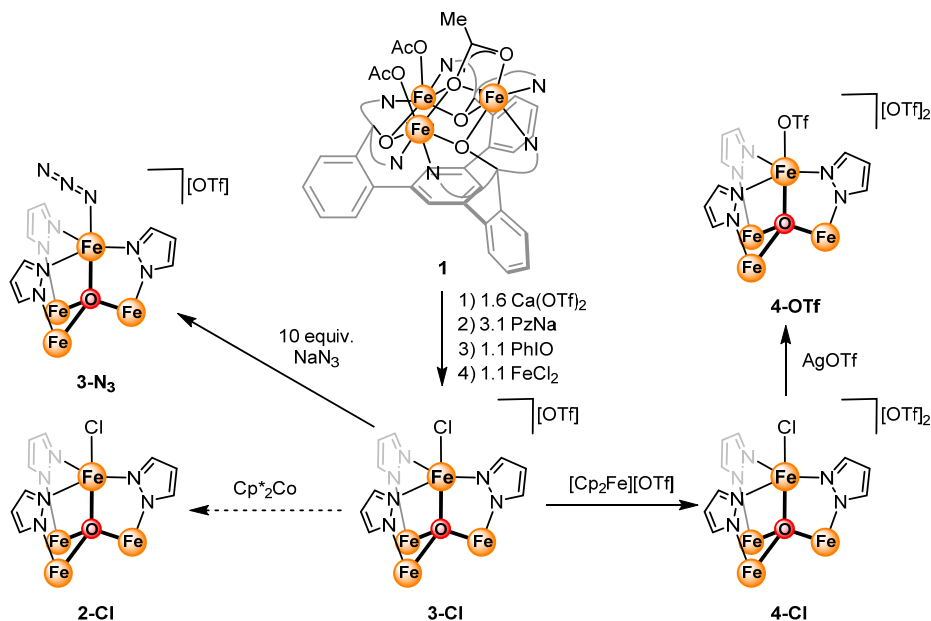


Section 5.2 Synthesis of [$\text{Fe}_4(\mu_4\text{-O})$] Complexes Supported by Parent Pyrazolate

Initial studies were carried out with parent pyrazole to access a less sterically crowded environment around the apical Fe and promote intermolecular reactivity and the coordination of small molecules. Initial syntheses involved the non-oxidative installation of the pyrazolates and apical Fe center from a cationic [$\text{Fe}^{\text{III}}_3(\mu_3\text{-O})\text{Cl}_3$] complex discussed in Appendix A. However, the reaction was sluggish and yielded inconsistent results despite the initial success on smaller scales. The optimized synthetic route involved the use of an oxidative route starting from the previously reported $\text{Fe}^{\text{II}}_3(\text{OAc})_3$ complex, **1**,¹³ more akin to strategies utilized in the reported pyrazolate-supported complexes.¹¹ The use of methyl triflate to remove acetates as reported for

phenylpyrazolate-supported clusters yielded messy reaction mixtures that were difficult to purify. Consequently, the use of alternative methods of acetate removal were pursued.

Scheme 2. Synthesis of $[\text{Fe}_4(\mu_4\text{-O})]$ clusters supported by pyrazolate



Preliminary results had shown that the synthesis of $[\text{Fe}_4(\mu_4\text{-O})]$ clusters supported by phenyl pyrazolate ligands from the previously reported calcium oxo hydroxo cluster was possible. Additionally, acetate removal from **1** with calcium triflate to produce a $[\text{Fe}^{\text{II}}_3(\text{OAc})_2(\text{OTf})]$ complex has also been described. Therefore, the use of calcium triflate as an acetate sink was explored. Gratifyingly, this approach proved successful to reproducibly access the desired $[\text{Fe}_4(\mu_4\text{-O})]$ complex, **3-Cl**, in a one-pot procedure. Calcium triflate addition to **1** in THF resulted in the *in situ* formation of a $[\text{Fe}^{\text{II}}_3(\text{OAc})_2(\text{OTf})]$ complex as a yellow/brown suspension. The subsequent addition of sodium pyrazolate resulted in the formation of a homogeneous red/orange solution. The addition of iodosylbenzene (PhIO) resulted in the formation of a brown solution, which is presumably the $[\text{Fe}_3\text{Na}(\mu_4\text{-O})]$ cluster by analogy to previously reported

syntheses. Installation of the apical Fe center could then be accomplished utilizing FeCl_2 . The calcium salts proved more readily removed due to their lower solubility in DCM thus allowing for the clean isolation of **3-C1** as a brown powder. Electrospray ionization mass spectrometry (ESI-MS) provided mixed results for these clusters likely attributable to the decreased steric protection and moisture and oxygen sensitivity.

Crystals suitable for single crystal X-ray diffraction (XRD) studies were obtained for **3-C1** (Figure 3). In the solid-state, **3-C1** displays a structure reminiscent of the phenylpyrazolate-supported clusters previously reported by our group with the Fe_3 core bridged to the apical Fe center by the (μ_4 -O) and pyrazolate ligands. The apical Fe center is 5-coordinate, likely to the reduced steric protection without the phenyl substituents, with a terminal chloride ligand trans to the (μ_4 -O). A τ_5 parameter of 0.968 for the apical Fe center indicates a trigonal bipyramidal geometry. Fe-(μ_4 -O) distances to the Fe_3 core are consistent with an $[\text{Fe}^{\text{III}}\text{Fe}^{\text{II}}_2]$ assignment with two longer (2.071(4), 2.145(3) Å) and one shorter (2.024(4) Å) distances. These data suggest that chloride coordination to the apical Fe center is sufficient to induce a redox rearrangement compared to other reported $[\text{Fe}^{\text{III}}_4\text{Fe}^{\text{II}}_2(\mu_4\text{-O})]$ clusters, which show localization of an apical Fe^{II} center in the apical position in four and five coordinate geometries. This is likely attributable to the anionic charge of the chloride ligand, a hypothesis that is supported by the localization of an apical Fe^{III} center in $[\text{Fe}_4(\mu_4\text{-O})]$ clusters with chelating phenoxide pyrazolate ligands.

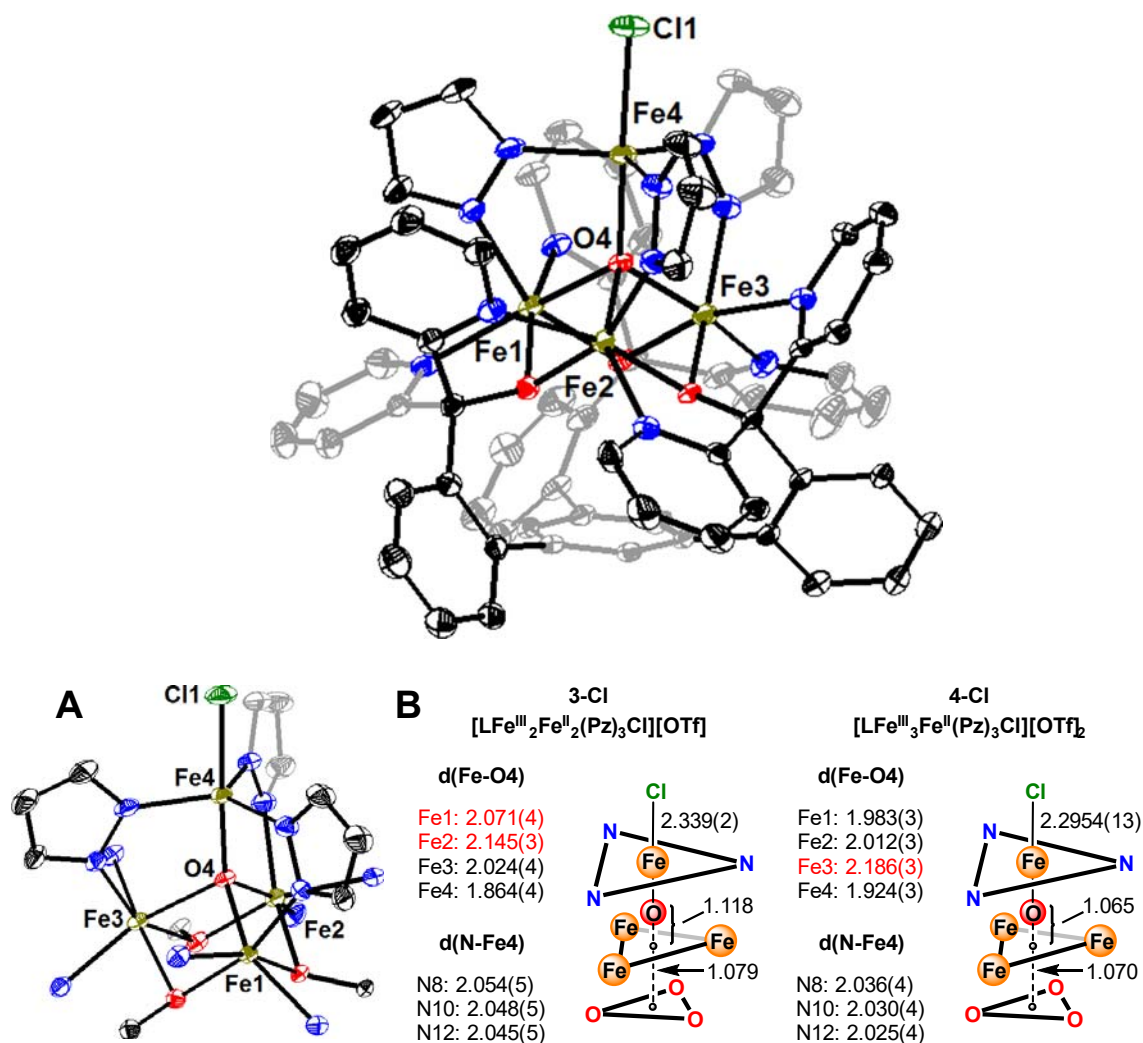


Figure 3. Solid-state structure **3-Cl** (top), and the truncated the $[\text{Fe}_4(\mu_4\text{-O})]$ core of **3-Cl** (A). Select bond metrics for **3-Cl** (B, Left) and **4-Cl** (B, Right). Hydrogen atoms, counterions, solvent molecules, and most of the supporting tris(alkoxide) hexa(pyridyl) ligand have been omitted for clarity.

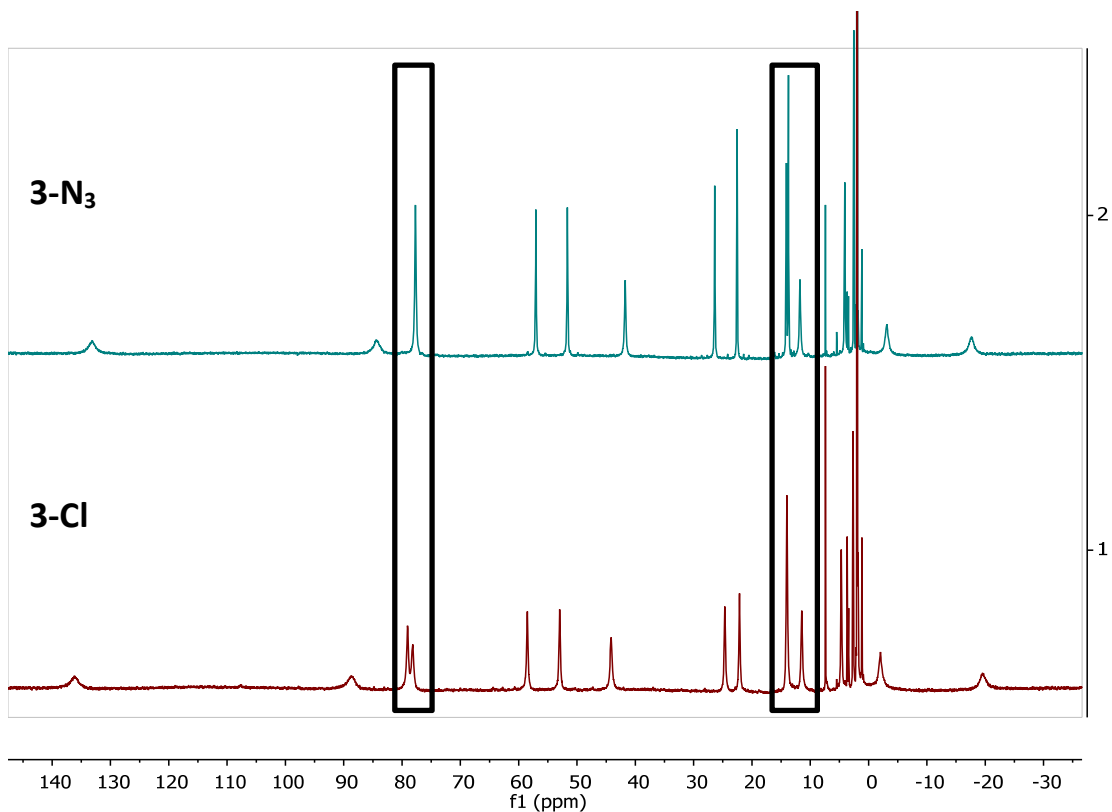


Figure 4. Comparison of NMR spectra for **3-Cl** (red trace) and **3-N₃** (blue trace) in CD₃CN. Boxed regions highlight the largest distinguishing features resulting from chloride substitution.

Substitution of the apical chloride was attempted. The addition of an excess of sodium azide yielded the desired terminal azide compound, **3-N₃** (Scheme 2). Confirmation of the presence of the azide ligand was confirmed by infrared (IR) spectroscopy, which showed an absorption at 2060 cm⁻¹. This stretch is more activated than in sodium azide (2129 cm⁻¹)¹⁴ and comparable to another reported trigonal bipyramidal Fe^{III} terminal azide complex supported by an amine tris(thiolate) ligand (2048 cm⁻¹).¹⁵ By NMR spectroscopy, **3-N₃** appears quite similar to **3-Cl** (Figure 4) indicating there are no substantial structural or electronic differences between the two complexes. A preliminary solid-state structure (R1 = 39.35%) also supports the formation of a terminal azide complex (Figure 5). Attempts to photolyze **3-N₃** with a

75 W Xenon lamp did not result in decomposition of the terminal azide to an Fe-nitride and dinitrogen. Attempts to repeat these reactions in different cluster oxidation states with a more powerful lamp are currently being pursued.

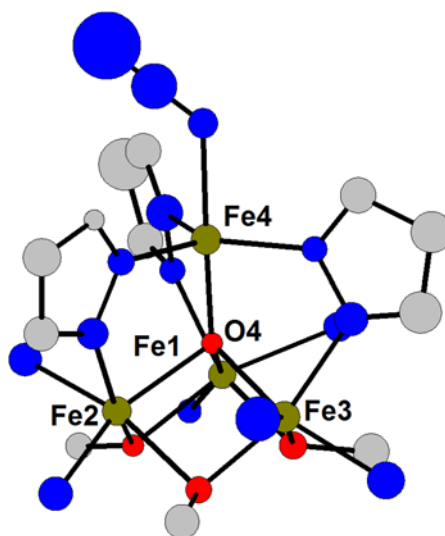


Figure 5. Preliminary solid-state structure of the $[\text{Fe}_4(\mu_4\text{-O})]$ core of **3-N₃**.

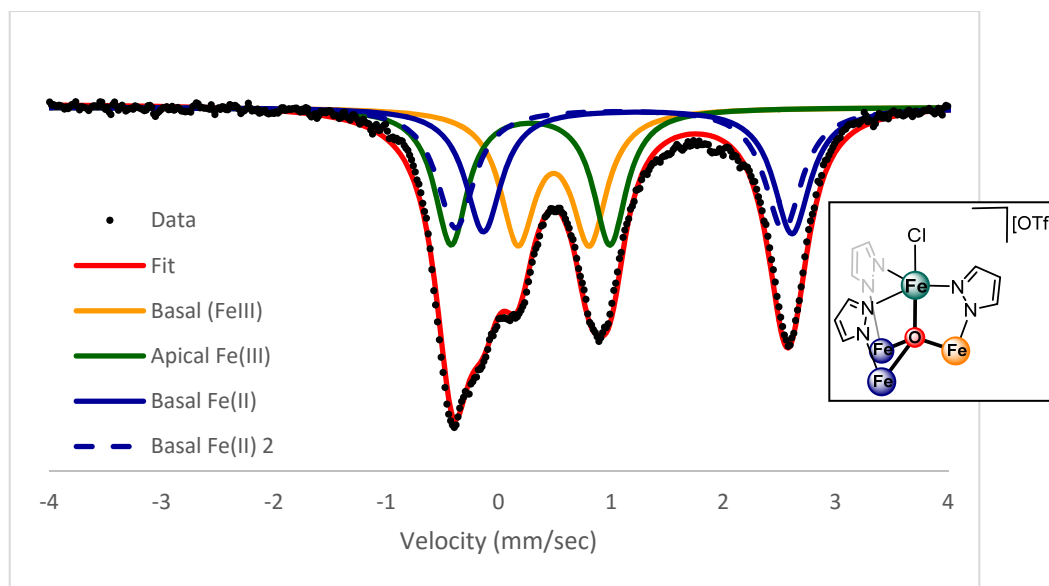


Figure 6. Zero-field ^{57}Fe Mössbauer spectrum at 80 K of **3-Cl** (black dots) and global fit (red trace) with simulated parameters (i) δ (mm/s) = 0.490, $|\Delta E_{\text{q}}|$ (mm/s) = 0.637 (blue trace); (ii) δ (mm/s) = 0.284, $|\Delta E_{\text{q}}|$ (mm/s) = 1.413 (orange trace); (iii) δ (mm/s) = 1.238, $|\Delta E_{\text{q}}|$ (mm/s) = 2.745 (green trace); (iv) δ (mm/s) = 1.076, $|\Delta E_{\text{q}}|$ (mm/s) = 2.915 (purple trace).

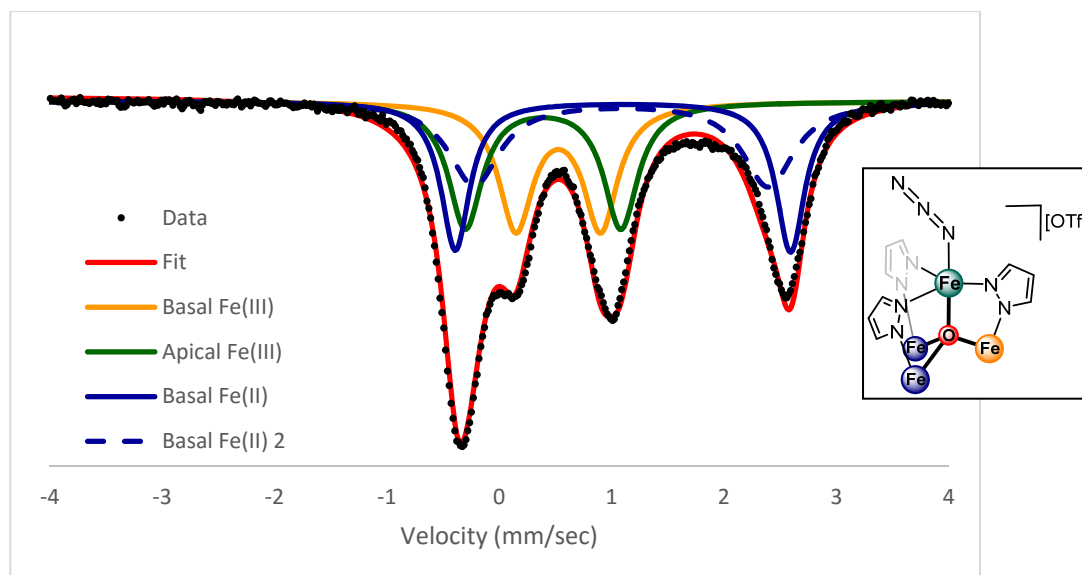


Figure 7. Zero-field ^{57}Fe Mössbauer spectrum at 80 K of **3-N₃** (black dots) and global fit (red trace) with simulated parameters (i) δ (mm/s) = 0.525, $|\Delta E_{\text{q}}|$ (mm/s) = 0.754 (blue trace); (ii) δ (mm/s) = 0.390, $|\Delta E_{\text{q}}|$ (mm/s) = 1.384 (orange trace); (iii) δ (mm/s) = 1.101, $|\Delta E_{\text{q}}|$ (mm/s) = 2.983 (green trace); (iv) δ (mm/s) = 1.084, $|\Delta E_{\text{q}}|$ (mm/s) = 2.615 (purple trace).

Mössbauer spectra were collected for **3-Cl** and **3-N₃** (Figure 6, 7) with simulated parameters summarized in Table 1. In both cases the data can be best fit as two Fe^{II} centers and two Fe^{III} centers. Based on the solid-state data for **3-Cl** and by comparison to previously synthesized phenoxide complexes in related clusters, the Fe^{III} component with the larger quadrupole splitting (Figure 5, 6 orange traces) was assigned as the apical Fe center for both complexes (**3-Cl** δ (mm/s): 0.284, $|\Delta E_{\text{q}}|$ (mm/s): 1.413; **3-N₃** δ (mm/s): 0.390, $|\Delta E_{\text{q}}|$ (mm/s): 1.384). Further support for this assignment comes from a pair of anionic monometallic Fe^{III} complexes supported by an amine tris(thiolate) ligand ($[\text{N}(\text{CH}_2\text{CH}_2\text{S})_3]^{3-}$). Both the $[\text{Et}_4\text{N}][\text{Fe}^{\text{III}}\text{Cl}(\text{NS}_3)]$ and $[\text{Et}_4\text{N}][\text{Fe}^{\text{III}}(\text{N}_3)(\text{NS}_3)]$ complex for this ligand were isolated with solid-state characterization confirming a trigonal bipyramidal 5-coordinate geometry akin to the apical Fe center in **3-Cl** and **3-N₃**. These complexes also have comparable reported

Mössbauer isomer shifts ($[\text{Et}_4\text{N}][\text{Fe}^{\text{III}}\text{X}(\text{NS}_3)]$: $\text{X} = \text{Cl}^-$ δ (mm/s): 0.258, $|\Delta E_{\text{q}}|$ (mm/s): 0.982; $\text{X} = \text{N}_3^-$ δ (mm/s): 0.352, $|\Delta E_{\text{q}}|$ (mm/s): 0.731). Furthermore, the trend of larger isomer shifts and smaller quadrupole splitting for the terminal azide compared to the chloride is reproduced in both pairs of complexes. Taken together these data all support the assignment of the apical Fe center as an Fe^{III} with an $[\text{Fe}^{\text{III}}\text{Fe}^{\text{II}}]$ core for both **3-Cl** and **3-N₃**.

Table 1. Summary of Mössbauer parameters for complexes **3-Cl** and **3-N₃**

Cmpd.	Formula	parameters		
		δ (mm/s)	$ \Delta E_{\text{q}} $ (mm/s)	%
3-Cl	$[\text{LFe}_3\text{OFe}(\text{Pz})_3\text{Cl}][\text{OTf}]$	0.490	0.637	25
		0.284	1.413	25
		1.238	2.745	25
		1.076	2.915	25
4-Cl	$[\text{LFe}_3\text{OFe}(\text{Pz})_3\text{Cl}][\text{OTf}]_2$	0.483	0.635	25
		0.320	0.679	25
		0.496	0.927	25
		1.086	2.946	25
3-N₃	$[\text{LFe}_3\text{OFe}(\text{Pz})_3(\text{N}_3)][\text{OTf}]$	0.525	0.754	25
		0.390	1.384	25
		1.101	2.983	25
		1.084	2.615	25
	$[\text{Et}_4\text{N}][\text{FeCl}(\text{NS}_3)]$	0.258	0.982	-
	$[\text{Et}_4\text{N}][\text{Fe}(\text{N}_3)(\text{NS}_3)]$	0.352	0.731	-

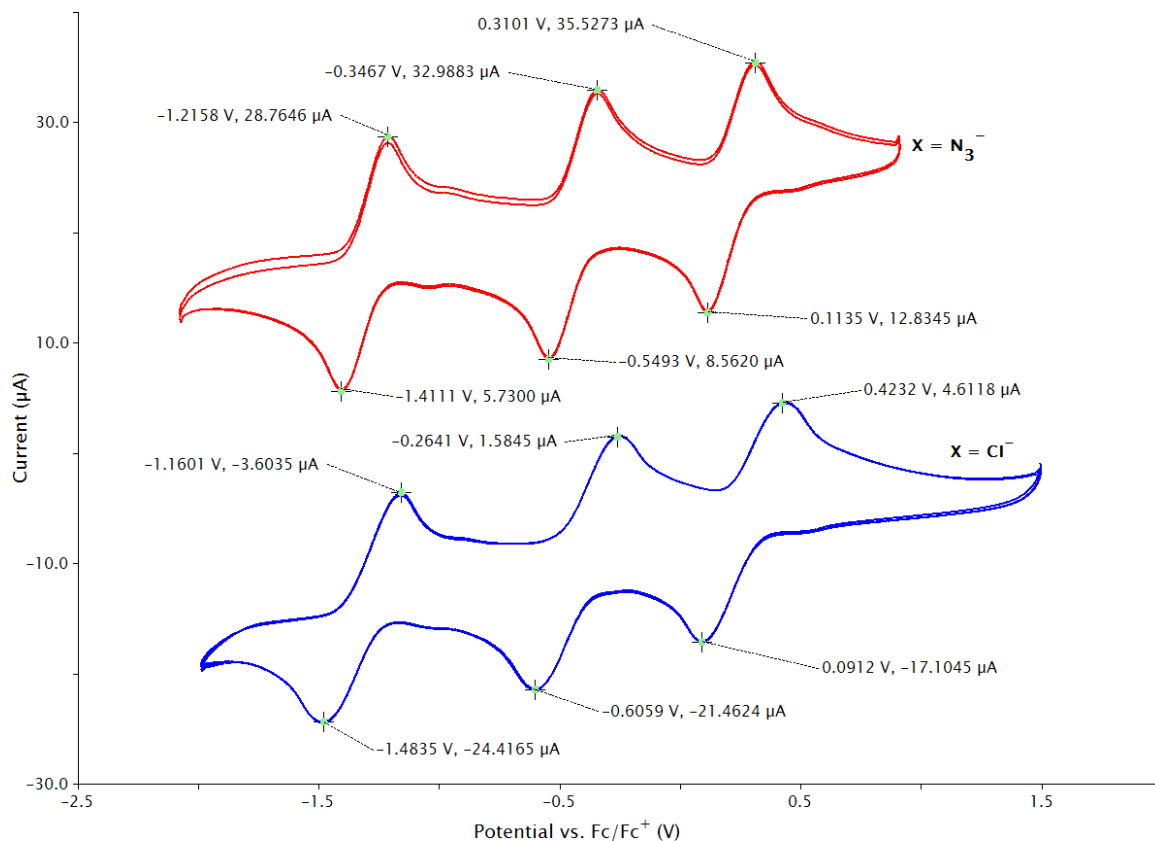


Figure 8. Stacked and normalized cyclic voltammograms (CVs) of **3-Cl** (blue trace) and **3-N₃** (red trace) in DCM at a scan rate of 100 mV/s. CVs were recorded a concentration of 2 mM and 1 mM for **3-Cl** and **3-N₃** respectively using a glassy carbon, platinum wire, and silver wire as working, counter, and reference electrodes respectively. 0.1 M [*n*Bu₄N][PF₆] was used as the supporting electrolyte.

Cyclic voltammetry (CV) studies of **3-Cl** and **3-N₃** were performed (Figure 8). Both complexes nearly identical electrochemical behavior with two quasireversible oxidations (**3-Cl**: -0.435, 0.26 V vs Fc/Fc⁺; **3-N₃**: -0.448, 0.22 V vs Fc/Fc⁺) corresponding to the [Fe^{III}₂Fe^{II}₂]/[Fe^{III}₃Fe^{II}] and [Fe^{III}₃Fe^{II}]/[Fe^{III}₄] couples respectively, and one quasireversible reduction (**3-Cl**: -1.32 vs Fc/Fc⁺; **3-N₃**: -1.31 V vs Fc/Fc⁺) corresponding to the [Fe^{III}₂Fe^{II}₂]/[Fe^{III}Fe^{II}₃] observable for both complexes. Compared to previously reported [Fe₄(μ₄-O)] clusters supported by phenylpyrazolate ligands, the oxidation to the [Fe^{III}₄] state is unusual. For both [LFe₄(μ₄-O)(PhPz)₃][OTf]₂ and

[LFe₄(μ₄-O)(NO)(PhPz)₃][OTf]₂ two reductions at (-1.733, -0.727 V vs Fc/Fc⁺) and (-1.662, -0.712 V vs Fc/Fc⁺) and one oxidation at 0.018 and 0.005 V vs Fc/Fc⁺ were observed for each complex respectively. While these complexes were reported to yield an [Fe^{II}₄] cluster utilizing decamethylcobaltocene as the reductant, no such oxidation state is electrochemically accessible with **3-Cl** or **3-N₃** in DCM. This suggests that chloride or azide coordination in **3-Cl** and **3-N₃** results in a significantly more electron-rich cluster that is substantially harder to reduce as seen from the shifts in the [Fe^{III}₂Fe^{II}₂]/[Fe^{III}Fe^{II}₃] ($\Delta E_{1/2} \sim -600$ mV) and [Fe^{III}₂Fe^{II}₂]/[Fe^{III}₃Fe^{II}] ($\Delta E_{1/2} \sim -450$ mV) couples relative to [LFe₄(μ₄-O)(NO)(PhPz)₃][OTf]₂ which also possesses a 5-coordinate apical Fe center.

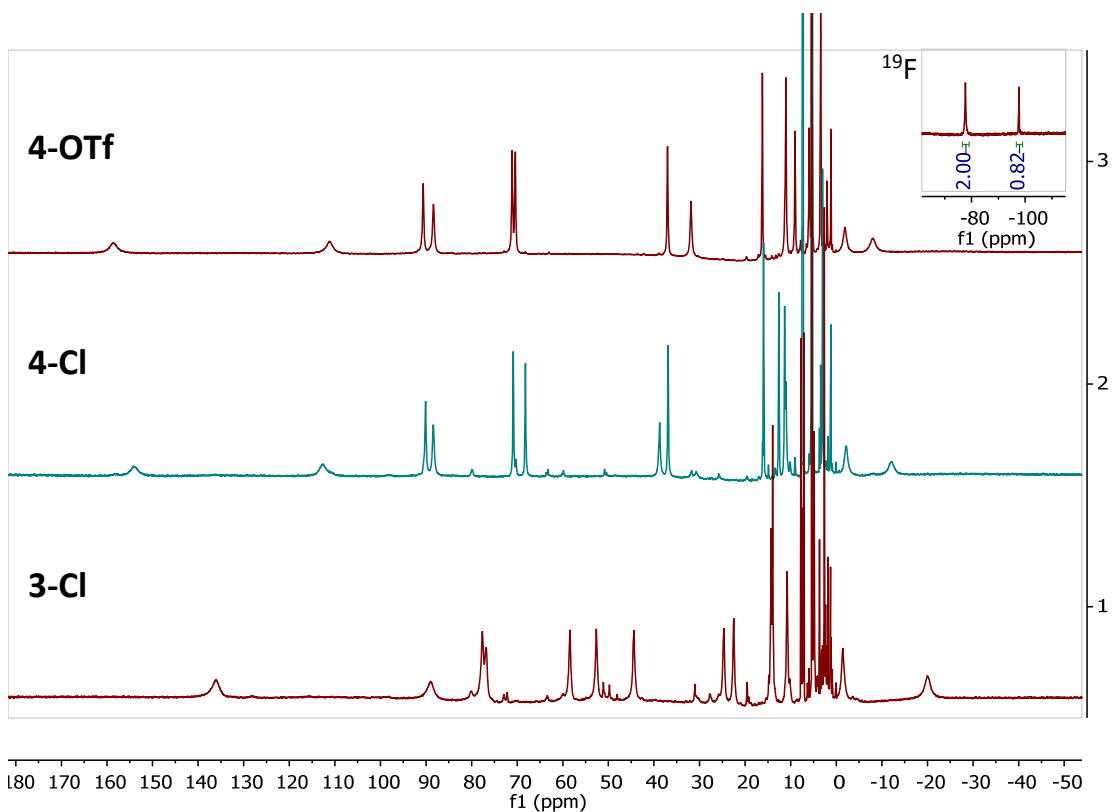


Figure 9. Comparison of NMR spectra for **3-Cl** (bottom red trace), **4-Cl** (blue trace), and **4-OTf** (top red trace) in CD₂Cl₂. Inset shows the ¹⁹F NMR spectra for **4-OTf**.

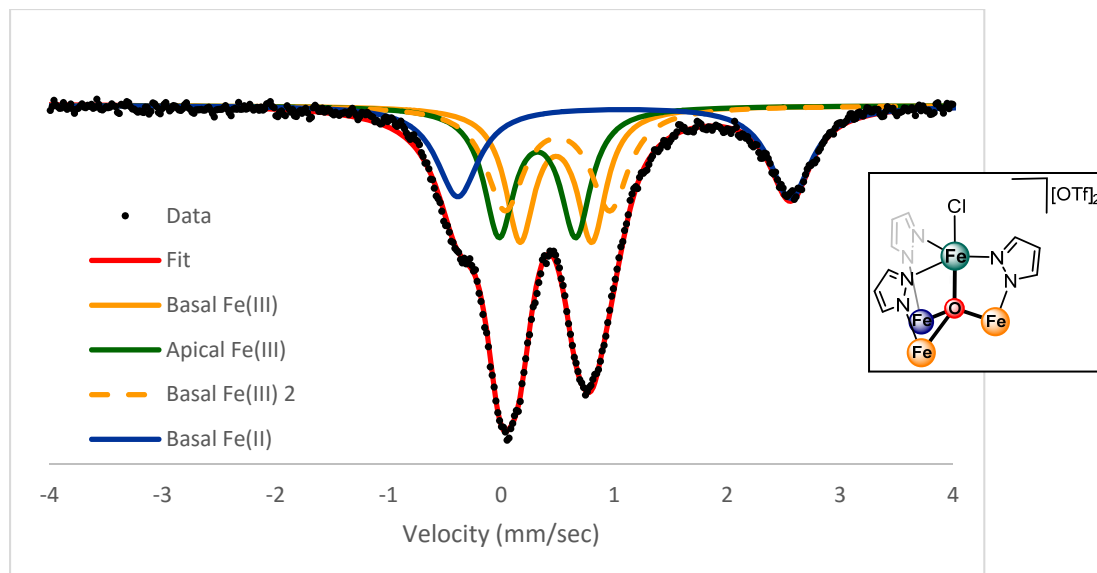


Figure 10. Zero-field ^{57}Fe Mössbauer spectrum at 80 K of **4-Cl** (black dots) and global fit (red trace) with simulated parameters (i) δ (mm/s) = 0.483, $|\Delta E_{\text{q}}|$ (mm/s) = 0.635 (blue trace); (ii) δ (mm/s) = 0.320, $|\Delta E_{\text{q}}|$ (mm/s) = 0.679 (orange trace); (iii) δ (mm/s) = 0.496, $|\Delta E_{\text{q}}|$ (mm/s) = 0.927 (green trace); (iv) δ (mm/s) = 1.086, $|\Delta E_{\text{q}}|$ (mm/s) = 2.946 (purple trace).

Attempts to isolate **3-Cl** in different oxidation states utilizing chemical oxidations and reductants was attempted. A clean oxidation with ferrocenium triflate was observed to yield the $[\text{LFe}^{\text{III}}_3\text{Fe}^{\text{II}}(\mu_4\text{-O})(\text{Pz})_3\text{Cl}][\text{OTf}]_2$ complex, **4-Cl** (Scheme 2). Substantial differences between **3-Cl** and **4-Cl** are observed by ^1H NMR spectroscopy (Figure 9). Single crystals suitable of XRD analysis were obtained for **4-Cl** (Figure 3). A comparable overall cluster geometry is observed for the one-electron oxidized complex. τ_5 parameter of 0.941 for the apical Fe center again indicates an approximately trigonal bipyramidal geometry. $\text{Fe}-(\mu_4\text{-O})$ distances to the Fe_3 core are now consistent with an $[\text{Fe}^{\text{III}}_2\text{Fe}^{\text{II}}]$ assignment with one longer (2.186(3) Å) and two shorter (1.983(3), 2.012(3) Å) distances. The O4-Fe_3 centroid distance shortens from 1.118 to 1.065 Å, which results in an elongation of the Fe4-O4 distance from 1.864(4) to 1.924(3) Å. Mössbauer data was also collected for **4-Cl** (Figure 10). **4-Cl** shows simulated parameters

summarized in Table 1. The data clearly indicates the presence of an $[\text{Fe}^{\text{III}}_3\text{Fe}^{\text{II}}]$ cluster confirming successful one-electron oxidation. This data is consistent with a formal oxidation of the Fe_3 core rather than an apical Fe-based redox process. Fe4-Cl and Fe4-N distances contract in **4-Cl**, likely to compensate for the decreased donor strength of the $(\mu_4\text{-O})$ to Fe4 as the Fe_3 core becomes more oxidized. Otherwise **3-Cl** and **4-Cl** remain largely isostructural as expected given the rigidity of the tris(pyrazole) supporting framework.

Attempts to reduce **3-Cl** yielded inconsistent results. Attempts to access the $[\text{Fe}^{\text{III}}_4]$ oxidation state of the cluster was attempted using silver triflate. In an NMR scale reaction halide abstraction rather than one electron oxidation appears to be the most consistent with the data. This is supported by the similarity of NMR features to the starting material (Figure 9) and the approximately 2:1 ratio of peaks observed in the ^{19}F NMR (Figure 9, inset) consistent with free triflate in solution with a single triflate coordinated the apical Fe center. The use of stronger metallocene-based oxidants is currently being pursued to access the $[\text{Fe}^{\text{III}}_4]$ cluster oxidation state without the risk of halide abstraction. Efforts to install terminal oxygenic fragments on **3-Cl** utilizing silver nitrite and tetrabutylammonium *meta*-periodate cleanly yielded **4-Cl** suggesting the use of **4-OTf** or another less coordinating ligand coordinated to the apical Fe center might be necessary for productive chemistry.

Section 5.3 Synthesis of $[\text{Fe}_4(\mu_4\text{-O})]$ Complexes with a Hydrogen Bonding Network

Efforts then turned to the synthesis of related clusters supported by pyrazolates capable of forming a hydrogen bonding network to moieties coordinated to the apical Fe center. Previous results with phenoxide pyrazole ligands and pyridine pyrazole indicated that both 5 and 6-member chelates from the pyrazolate were feasible.

Therefore the use of the 3-aminophenyl pyrazole ligand ((**PhNH**)**PzH**) was pursued due to the smaller, 4-member ring size which would likely prevent chelation. Analogous cluster construction procedures for **3-Cl** were utilized allowing for the isolation of the analogous $[\text{LFe}^{\text{III}}_2\text{Fe}^{\text{II}}_2(\mu_4\text{-O})(\text{PhNHPz})_3\text{Cl}][\text{OTf}]$ complex, **6-Cl**, in a one pot synthesis from **1** (Scheme 3). A preliminary solid-state structure obtained for the complex confirmed the connectivity of the tetranuclear core (Figure 11). While a detailed comparison of bond metrics is prohibited by the comparatively lower quality of the crystal structure ($R1 = 20.65\%$), a substantial elongation of the Fe–Cl bond distance ($\sim 2.68 \text{ \AA}$) has occurred compared to **3-Cl** ($2.339(2) \text{ \AA}$). This elongation is consistent with a previous report on a three-fold symmetric ligand capable of hydrogen bonding to a terminal Fe–Cl ligand.¹⁶ However, this Fe–Cl distance is unusually long though a better solid-state structure is required to support this claim. The three N–Cl distances for the aminophenyl moieties are all roughly 3 \AA long consistent with a hydrogen bonding interaction. Geometrically the three NH hydrogen bond donors are arranged in a nearly C_3 arrangement about the chloride ligand. As a consequence of the hydrogen bonding to the chloride, the ligand loses electron density and forms a weaker interaction with the Fe center.

The $[\text{Fe}^{\text{III}}_2\text{Fe}^{\text{II}}_2]$ oxidation state was confirmed by the Mössbauer data obtained for **6-Cl** (Figure 12). The apical Fe center has been assigned as the Fe^{III} component with the larger quadrupole splitting ($\delta \text{ (mm/s)} = 0.504$, $|\Delta E_{\text{q}}| \text{ (mm/s)} = 1.066$), however no Mössbauer data for comparable hydrogen bonded Fe–Cl moieties have been reported in the literature for structurally characterized complexes making confirmation of this assignment more tenuous. The remaining components of the Mössbauer

spectrum are comparable to reported parameters for Fe^{III} and Fe^{II} centers is related complexes (Table 2).

Scheme 3. Synthetic routes to $[\text{Fe}_4(\mu_4\text{-O})]$ clusters supported by **(PhNH)Pz** ligands

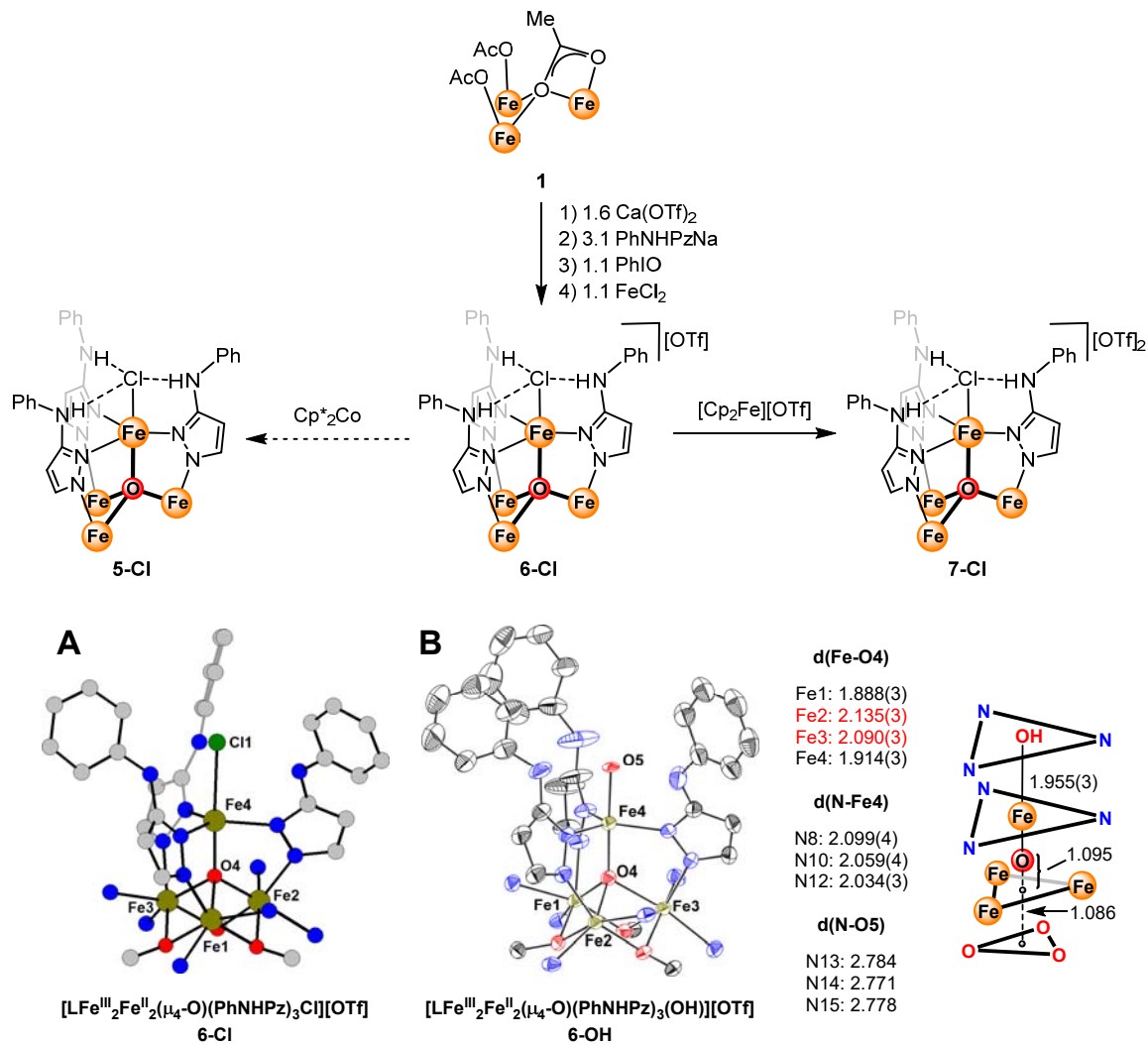


Figure 11. Solid-state structure of the $[\text{Fe}_4(\mu_4\text{-O})]$ core of **6-Cl** (A) and **6-OH** (B). Select bond metrics for **6-OH** (B, Right). Hydrogen atoms, counterions, solvent molecules, and most of the supporting tris(alkoxide) hexa(pyridyl) ligand have been omitted for clarity.

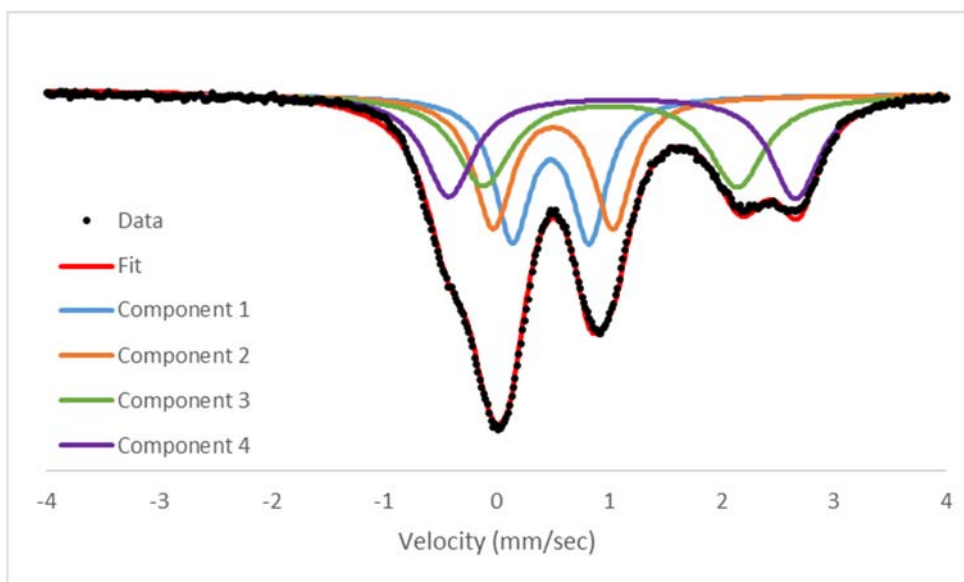


Figure 12. Zero-field ^{57}Fe Mössbauer spectrum at 80 K of **6-Cl** (black dots) and global fit (red trace) with simulated parameters (i) δ (mm/s) = 0.483, $|\Delta E_{\text{q}}|$ (mm/s) = 0.685 (blue trace); (ii) δ (mm/s) = 0.504, $|\Delta E_{\text{q}}|$ (mm/s) = 1.066 (orange trace); (iii) δ (mm/s) = 1.012, $|\Delta E_{\text{q}}|$ (mm/s) = 2.254 (green trace); (iv) δ (mm/s) = 1.118, $|\Delta E_{\text{q}}|$ (mm/s) = 3.080 (purple trace).

The electrochemical behavior of **6-Cl** in DCM was also studied using cyclic voltammetry experiments (Figure 13). While the sample was not entirely pure as evidenced by small shoulders on redox events, **6-Cl** also displays one quasireversible (-1.15 V vs Fc/Fc^+) reduction and two quasireversible oxidations (-0.42, 0.16 V vs Fc/Fc^+) again indicating chloride binding substantially shifts the redox potentials compared to $[\text{LFe}_4(\mu_4\text{-O})(\text{NO})(\text{PhPz})_3][\text{OTf}]_2$. Interestingly, despite the presence of electron-donating aminophenyl substituents compared to **3-Cl** there not appear to be a shift in reduction potentials to more negative values. In fact the reduction potential corresponding to the $[\text{Fe}^{\text{III}}_2\text{Fe}^{\text{II}}_2]/[\text{Fe}^{\text{III}}\text{Fe}^{\text{II}}_3]$ couple of **6-Cl** is actually approximately +150 mV more positive than **3-Cl**. However, the oxidation events corresponding to the $[\text{Fe}^{\text{III}}_2\text{Fe}^{\text{II}}_2]/[\text{Fe}^{\text{III}}_3\text{Fe}^{\text{II}}]$ and $[\text{Fe}^{\text{III}}_3\text{Fe}^{\text{II}}]/[\text{Fe}^{\text{III}}_4]$ couples respectively occur at similar (+10 mV) and lower (-98 mV) potentials. This suggests that at higher oxidation states the

electron-donating aminophenyl substituents do facilitate oxidation of the complex. At higher potentials ~ 0.6 V vs Fc/Fc⁺ another irreversible oxidation is observed, however this could correspond to a ligand oxidation of one of the aminophenyl substituents rather than a [Fe^{III}₄]/[Fe^{IV}Fe^{III}₃] couple. However, further characterization of this third oxidation event is required.

Table 2. Summary of Mössbauer parameters for complex **6-Cl**

Cmpd.	Formula	parameters		
		δ (mm/s)	$ \Delta E_q $ (mm/s)	%
4	[LFe ₃ OFe(PhNHPz) ₃ Cl][OTf]	0.483	0.685	25
		0.504	1.066	25
		1.012	2.254	25
		1.118	3.080	25

Attempts to chemically access different redox states of **6-Cl** was attempted. Much like **3-Cl**, the reduction of **5-Cl** proved sluggish and provided inconsistent results. However, the addition of ferrocenium triflate resulted in the formation of the one electron oxidized complex, **7-Cl** (Scheme 3). Solution NMR indicates, **7-Cl** looks quite distinct from **6-Cl** (Figure 14). Future attempts to access the [Fe^{III}₄] complex will be made. Solid-state characterization and Mössbauer spectroscopy will be pursued to better assess differences that arise upon one-electron oxidation of the [Fe₄(μ_4 -O)] core.

A serendipitous result was obtained from attempts to synthesize [Fe₄(μ_4 -O)]-type clusters using Fe(OTf)₂ rather than FeCl₂ as the fourth equivalent of Fe. With older batches of Ca(OTf)₂ and PhIO, the formation of a new species by NMR that was later confirmed to the a terminal hydroxide moiety by XRD analysis was observed (Figure 11). The Fe–O(H) distance of 1.955(3) Å is consistent with comparable species in the literature stabilize by hydrogen bonding interactions.^{10a, 17} Fe–O4 distances to the Fe₃ core are consistent with an [Fe^{III}Fe^{II}₂] assignment as evidenced with the two long

(2.135(3), 2.090(3) Å) and one short (1.888(3) Å) bond length. A distortion from the pseudo- C_3 -fold symmetric distribution of the aminophenyl hydrogen bond donors is observed consistent with the assignment as a hydroxo ligand.

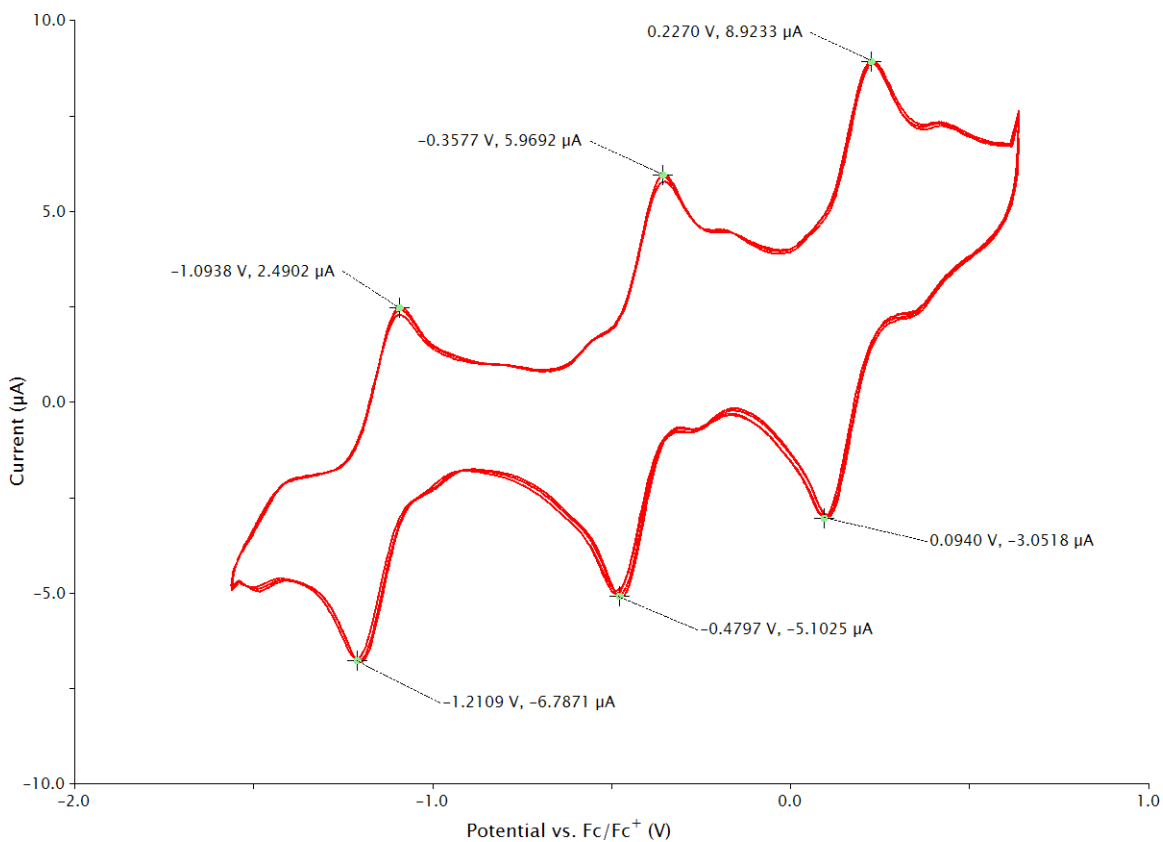


Figure 13. Cyclic voltammogram (CV) data for **6-Cl** (red trace) in DCM at a scan rate of 50 mV/s. CVs were recorded at a concentration of 1 mM using a glassy carbon, platinum wire, and silver wire as working, counter, and reference electrodes respectively. 0.1 M $[n\text{Bu}_4\text{N}][\text{PF}_6]$ was used as the supporting electrolyte.

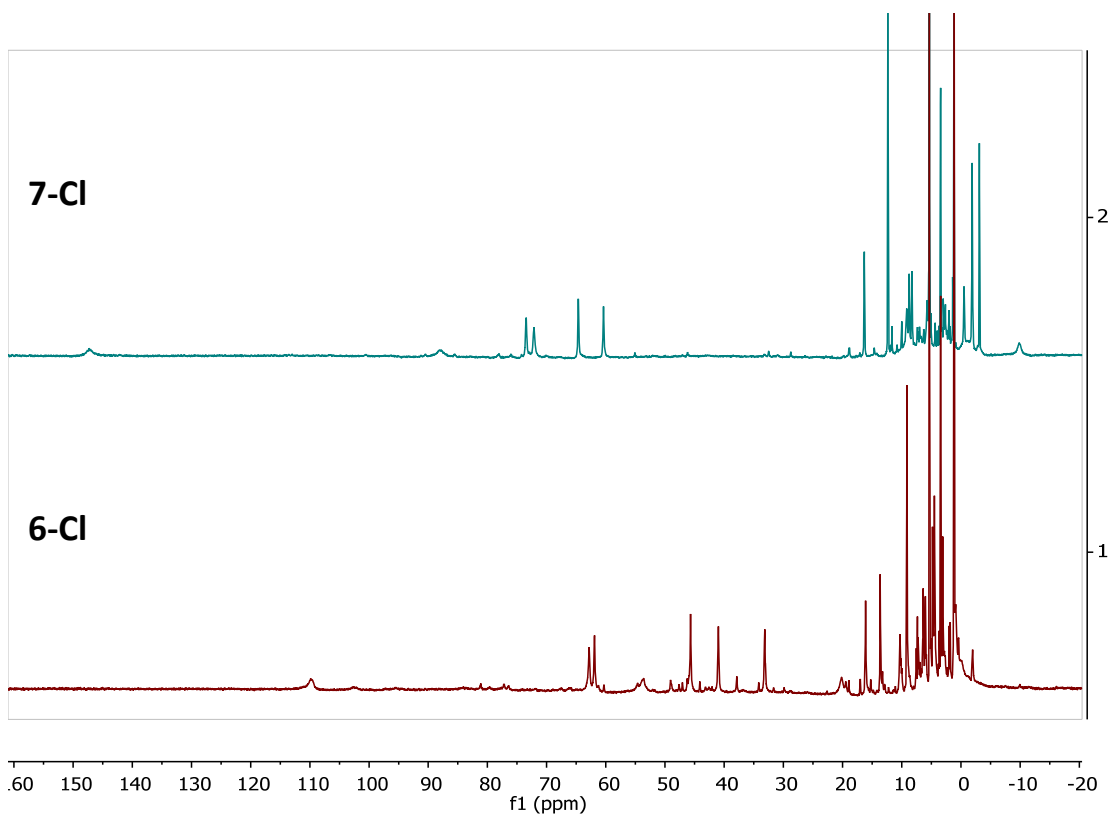
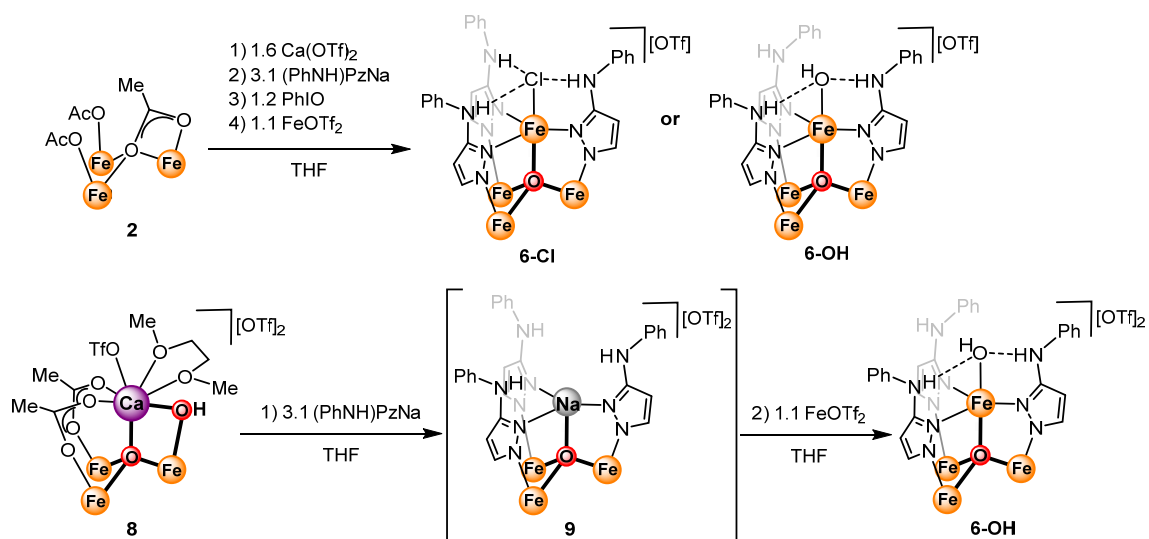


Figure 14. ^1H NMR comparison for **6-Cl** (red trace) and **7-Cl** (blue trace) in CD_2Cl_2 .

Scheme 4. Synthesis of $[\text{Fe}_4(\mu_4\text{-O})]$ clusters with a terminal hydroxide ligand



However, efforts to reproducibly synthesize **6-OH** from **1** proved challenging. Depending on the source starting materials **6-Cl** was observed to be the majority

species produced on multiple occasions. As the source of the terminal hydroxide ligand is likely from adventitious water or hydroxide impurities coordinated to the calcium or iron triflate precursors, efforts to rationally synthesize **6-OH** from alternative precursors was pursued. A previously reported $[\text{Fe}_3\text{Ca}(\mu_4\text{-O})(\mu_2\text{-OH})]$ complex was utilized as a precursor as both the oxo and hydroxo ligand content need to synthesize **6-OH** is already present in the precursor. This route proved successful on smaller scales though incomplete transmetalation was often observed in reactions. Future efforts will focus on the scaling up of this route. Additionally, efforts to utilize salt metathesis routes to convert **6-Cl** into **6-OH** with precursors such as $[\text{NMe}_4][\text{OH}]$, KOH , or NaOH will also be pursued. Once reproducible routes to **6-OH** are established, efforts will turn to the stabilization of terminal oxo species utilizing the stabilizing effects of the hydrogen bonding network provided by the **(PhNH)PzH** ligands.

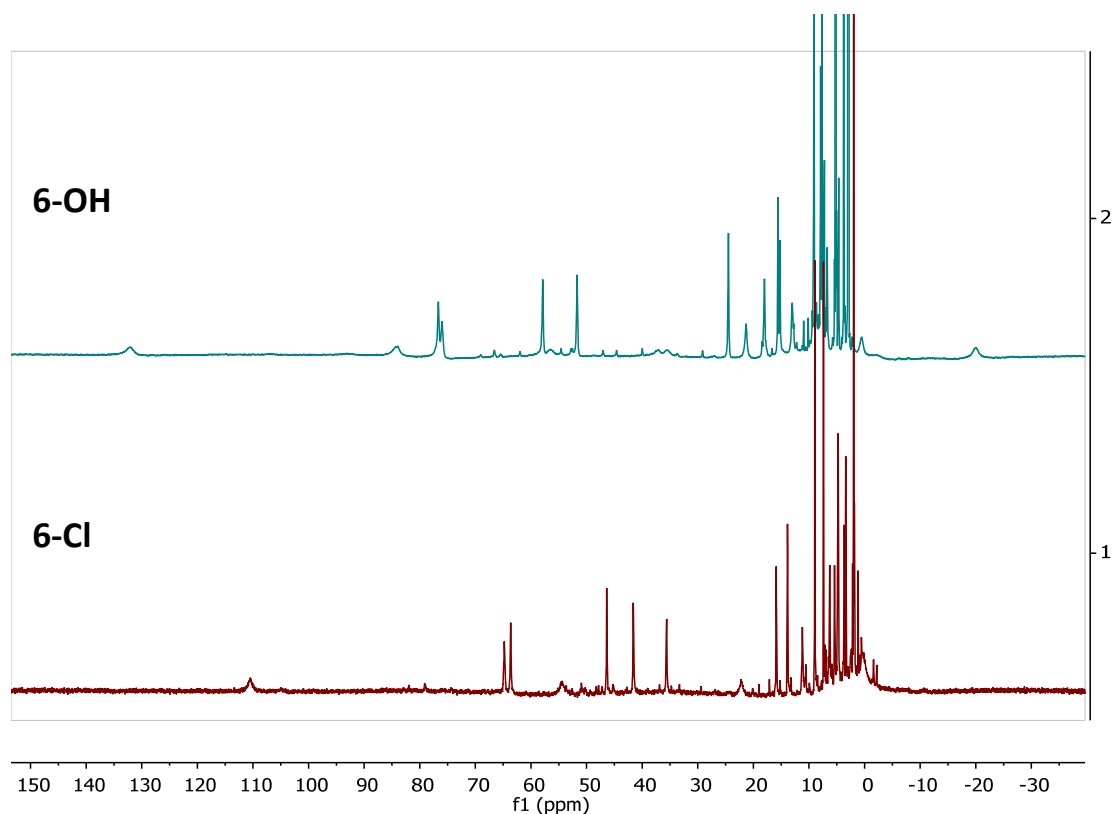
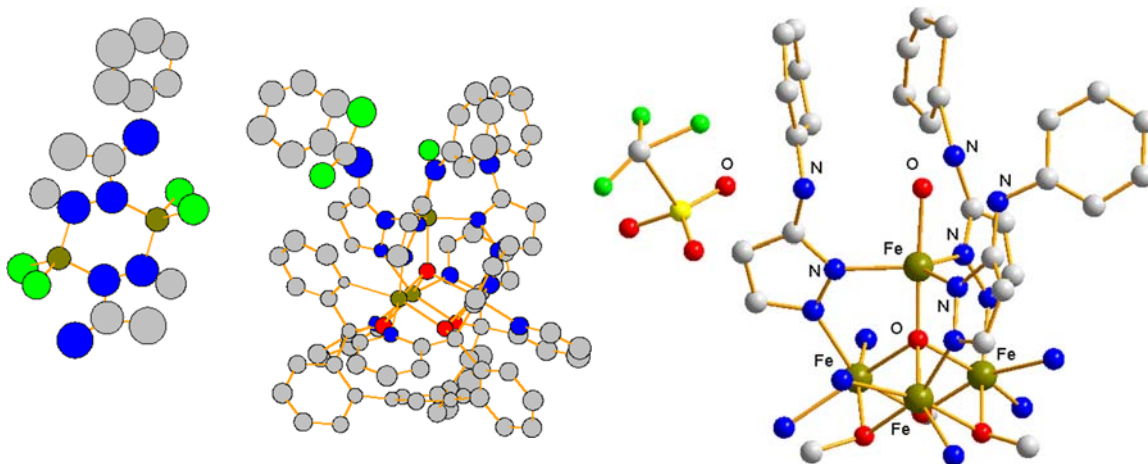


Figure 14. ^1H NMR comparison for **6-Cl** (red trace) and **6-OH** (blue trace) in CD_3CN .

Section 5.4 Miscellaneous Crystal Structures



CONCLUSIONS

In conclusion, two new pyrazolate ligands have been explored study the effect of reduced steric bulk and hydrogen bonding networks on the small molecule activation reactivity of site-differentiated $[\text{Fe}_4(\mu_4\text{-O})]$ clusters. The reduction of steric bulk allows access to terminal chloride complexes where the apical Fe center prefers the Fe^{III} oxidation state rather than Fe^{II} as seen with reported clusters. With the parent pyrazolate ligand, clean substitution of the chloride ligand for azide can be observed. Mössbauer parameters for the apical Fe center are in good agreement with previously reported literature complexes. Efforts to construct hydrogen bonding networks surrounding the apical Fe center have also proven successful. Compared the **3-Cl** and **4-Cl**, preliminary solid-state structures obtained for **6-Cl** shows an unusually long Fe–Cl bond consistent with hydrogen bonding from all three aminophenyl NH moieties to the chloride ligand. This unusually long elongation may also be attributable to the unusual stability of these pyrazolate-supported scaffolds to stabilize coordinatively-

unsaturated, 4-coordinate apical Fe centers using phenyl pyrazolate ligands. Efforts to synthesize terminal oxo and hydroxo moieties in a rational fashion are currently under development in the group.

EXPERIMENTAL SECTION

General considerations.

Unless otherwise specified, all air- and moisture-sensitive compounds were manipulated using glovebox or using standard Schlenk line techniques with an N₂ atmosphere. Anhydrous tetrahydrofuran (THF) was purchased from Aldrich in 18 L Pure-Pac™ containers. Anhydrous pentanes, hexanes, benzene, toluene, diethyl ether, and THF were purified by sparging with nitrogen for 15 minutes and then passing under nitrogen pressure through a column of activated A2 alumina (Zapp's).¹⁸ Benzene-*d*₆, tetrahydrofuran-*d*₈, and acetonitrile-*d*₃ was purchased from Cambridge Isotope Laboratories, Inc., dried over sodium/benzophenone ketyl (benzene and THF) or calcium hydride (MeCN) and vacuum transferred prior to use. Unless indicated otherwise, all commercial chemicals were used as received. ¹H, ¹³C, and ³¹P NMR spectra were recorded on Varian Mercury 300 or Varian INOVA-500 spectrometers at room temperature unless indicated otherwise. Chemical shifts for ¹H and ¹³C NMR data are reported relative to residual solvent peaks and are decoupled with respect to each other unless otherwise noted.¹⁹ Powder and thin film ATR-IR measurements were obtained by placing a powder or drop of solution of the complex on the surface of a Bruker APLHA ATR-IR spectrometer probe and allowing the solvent to evaporate (Platinum Sampling Module, diamond, OPUS software package) at 2 cm⁻¹ resolution. **(PhNH)PzH**¹² and **1**¹³ were synthesized according to literature procedures.

Synthesis of Complex 3-Cl

Compound **1** (300 mg, 0.250 mmol, 1 equiv) and calcium triflate (135.2 mg, 0.400 mmol, 1.6 equiv) were transferred to a Schlenk tube fitted with a screw-in Teflon stopper and

equipped with a magnetic stirbar. THF (*ca.* 20 mL) were then added the combined mixture was allowed to stir for 1 hr during which time the solution changed from an orange suspension to a yellow-brown suspension. Sodium pyrazolate (67.5 mg, 0.750 mmol, 3 equiv) was then added as a solution in *ca.* 5 mL THF. The reaction mixture immediately turned a deep red color and became more homogeneous and was allowed to stir for 2 hrs. Iodosylbenzene (55.0 mg, 0.250 mmol, 1 equiv) was then added as a suspension in THF (*ca.* 5 mL). The reaction mixture was allowed to stir for 3 hrs during which time the solution became brown. FeCl₂ (34.8 mg, 0.275 mmol, 1.1 equiv) was then added as a suspension in THF (*ca.* 5 mL) and the reaction mixture was allowed to stir for 16 hrs. Reaction volatiles were then removed under reduced pressure. The residue was washed with DCM and filtered through a Celite pad until washes became clear to remove salts. Volatiles from the filtrate were then removed under reduced pressure to yield **3-Cl** as a brown powder. Yield: 317.5 mg (87 %). ¹H NMR (300 MHz, CD₃CN) δ 137.35 (s, 1H), 89.43 (s, 1H), 79.77 (s), 78.92 (s), 59.05 (s), 53.43 (s), 44.69 (s), 24.52 (s), 22.32 (s), 14.07 (s), 11.53 (s), -2.07 (s), -19.99 (s). ¹⁹F NMR (282 MHz, CD₃CN) δ -79.28. ⁵⁷Fe Mössbauer: δ (mm/s) (|ΔE_q| (mm/s)): 0.490 (0.637), 0.284 (1.413), 1.238 (2.745), 1.076 (2.915).

Synthesis of Complex **3-N₃**

Complex **3-Cl** (106.9 mg, 0.066 mmol, 1 equiv) was transferred to a 20 mL scintillation vial equipped with a magnetic stirbar. Sodium azide (43.1 mg, 0.660 mmol, 10 equiv) was then added as a suspension in THF (*ca.* 5 mL). The combined reaction mixture was allowed to stir for 16 hrs. Reaction volatiles were then removed under reduced pressure. The residue was washed with DCM and filtered through a Celite pad until washes became colorless. Volatiles

from the filtrate were then removed under reduced pressure yielding the product as a brown solid. Yield: 80 mg (75 %). ^1H NMR (300 MHz, CD_3CN) δ 134.98 (s), 85.41 (s), 78.71 (s), 57.78 (s), 52.28 (s), 42.41 (s), 26.25 (s), 22.79 (s), 14.18 (s), 13.84 (s), 11.84 (s), -3.25 (s), -18.16 (s). ^{19}F NMR (282 MHz, CD_3CN) δ -79.31. IR: $\nu(\text{N}_3)$: 2060 cm^{-1} . ^{57}Fe Mössbauer: δ (mm/s) ($|\Delta E_q|$ (mm/s)): 0.525 (0.754), 0.390 (1.384), 1.101 (2.983), 1.084 (2.615).

Synthesis of Complex 4-Cl

Complex **3-Cl** (106.9 mg, 0.069 mmol, 1 equiv) was transferred to a 20 mL scintillation vial equipped with a magnetic stirbar. Ferrocenium triflate (23.2 mg, 0.069 mmol, 1 equiv) was then added as a solution in *ca.* 5 mL of DCM. The reaction mixture was allowed to stir for 1 hr. Reaction volatiles were then removed under reduced pressure. The residue was washed with benzene and filtered through a Celite pad to remove the majority of the ferrocene byproduct. The residue was then washed with DCM to elute the product. The volatiles of the DCM filtrate were then removed under reduced pressure. The obtained product was then recrystallized from a DCM: Et_2O vapor diffusion yielding the product as a brown precipitate. Yield: 101 mg (86 %). ^1H NMR (300 MHz, CD_2Cl_2) δ 154.10 (s), 112.63 (s), 90.11 (s), 88.40 (s), 70.87 (s), 68.20 (s), 38.78 (s), 36.90 (s), 15.95 (s), 12.62 (s), 11.32 (s), 11.04 (s), -2.16 (s), -12.07 (s). ^{19}F NMR (282 MHz, CD_2Cl_2) δ -77.96. ^{57}Fe Mössbauer: δ (mm/s) ($|\Delta E_q|$ (mm/s)): 0.483 (0.635), 0.320 (0.679), 0.496 (0.927), 1.086 (2.946).

Synthesis of Complex 6-Cl

Compound **1** (700 mg, 0.583 mmol, 1 equiv) and calcium triflate (317 mg, 1.75 mmol, 1.6 equiv) were transferred to a Schlenk tube fitted with a screw-in Teflon stopper and equipped with a magnetic stirbar. THF (*ca.* 40 mL) were then added the combined mixture was allowed to stir for 1 hr during which time the solution changed from an orange suspension to a yellow-brown suspension. **(PhNH)PzNa** (317 mg, 1.75 mmol, 3 equiv) was then added as a solution in *ca.* 5 mL THF. The reaction mixture immediately turned a deep red color and became more homogeneous and was allowed to stir for 2 hrs. Iodosylbenzene (128.3 mg, 0.583 mmol, 1 equiv) was then added as a suspension in THF (*ca.* 5 mL). The reaction mixture was allowed to stir for 3 hrs during which time the solution became a deep purple. FeCl₂ (81.3 mg, 0.641 mmol, 1.1 equiv) was then added as a suspension in THF (*ca.* 5 mL) and the reaction mixture was allowed to stir for 16 hrs. During this time the reaction mixture change color from purple to a blue/purple color. Reaction volatiles were then removed under reduced pressure. The residue was washed with DCM and filtered through a Celite pad until washes became clear to remove salts. Volatiles from the filtrate were then removed under reduced pressure to yield mostly pure **6-Cl** as a blue/purple powder. Yield: 750 mg (73 %). During purification attempts, it was found dissolving this material in acetonitrile and filtering through a second Celite pad afforded clean **6-Cl** suitable for further analysis. However, much of the material had been split between different purification protocols making an accurate estimate a yield via this method challenging. ¹H NMR (300 MHz, CD₃CN) δ 110.86 (s), 65.12 (s), 63.95 (s), 46.55 (s), 41.69 (s), 35.66 (s), 22.54 (s), 15.97 (s), 13.89 (s), 11.26 (s). ¹⁹F NMR (282 MHz, CD₃CN) δ -79.30. ⁵⁷Fe Mössbauer: δ (mm/s) (|ΔE_q| (mm/s)): 0.483 (0.685), 0.504 (1.066), 1.012 (2.254), 1.118 (3.080).

Synthesis of Complex 7-Cl

Complex **6-Cl** (80 mg, 0.046 mmol, 1 equiv) was transferred to a 20 mL scintillation vial equipped with a magnetic stirbar. Ferrocenium triflate (15.3 mg, 0.046 mmol, 1 equiv) was then added as a solution in *ca.* 5 mL of DCM. The reaction mixture was allowed to stir for 1 hr. During this time a color change from blue to green/blue was observed. The reaction mixture was concentrated (*ca.* 1 mL) under reduced pressure and then Et₂O (*ca.* 20 mL) was added to precipitate the product. The reaction mixture was filtered onto a Celite pad and washed with Et₂O until the filtrate became colorless. The residue was then washed with DCM to elute the product. The volatiles of the DCM filtrate were then removed under reduced pressure. The obtained product was then recrystallized from a DCM:Et₂O vapor diffusion yielding the product as a brown precipitate. Yield: 71.7 mg (83 %). ¹H NMR (300 MHz, CD₂Cl₂) δ 147.38 (s), 88.11 (s), 73.48 (s), 72.16 (s), 64.65 (s), 60.41 (s), 16.33 (s), 12.34 (s), -9.87 (s). ¹⁹F NMR (282 MHz, CD₂Cl₂) δ -76.74.

Mössbauer Details

Zero-field ⁵⁷Fe Mössbauer spectra were recorded at 80 K in the constant acceleration mode on a spectrometer from See Co (Edina, MN) equipped with an SVT-400 cryostat (Janis, Wilmington, WA). The quoted isomer shifts are relative to the centroid of the spectrum of a α -Fe foil at room temperature. Samples were prepared by grinding polycrystalline material (20 mg) into a fine powder and pressed into a homogeneous pellet with boron nitride in a cup fitted with a screw cap. The data were fitted to Lorentzian lineshapes using the program WMOSS (www.wmoos.org).

Mössbauer simulation details for compounds 3-Cl, 3-N₃, 4-Cl, and 6-Cl.

All spectra were simulated by four pairs of symmetric quadrupole doublets with equal populations and Lorentzian lineshapes, and refined to a minimum by the method of least squares optimization (a total of 13 fitting parameters per spectrum). For all spectra, the observed resonances spanned the region from -1–3 mm s⁻¹. Any resonances appearing above 2 mm s⁻¹ indicate the presence of high spin Fe(II) centers and must correspond to species with isomer shifts ~1 mm s⁻¹, given the range of observed resonances. In short, the Mössbauer data were modeled to be consistent with our previously reported triiron-oxo/hydroxyl clusters,⁸ and our previously reported tetranuclear iron clusters.²

Table 1. Crystal and refinement data for reported complexes.

Complex	3-Cl	4-Cl	6-OH
empirical formula	C ₇₉ H ₄₈ ClF ₃ Fe ₄ N ₁₂ O ₁₀ S	C ₇₂ H ₅₅ ClF ₅ Fe ₄ N ₁₃ O 11S ₂	C _{96.60} H _{77.19} F ₃ Fe ₄ N ₁₅ O _{10.77} S
formula wt	1673.20	1696.26	1933.04
T (K)	99.97	100.01	100.0
a, Å	12.4451(10)	12.2975(7)	17.2031(6)
b, Å	26.739(2)	17.0691(10)	17.6939(5)
c, Å	24.0447(18)	18.4705(11)	18.0034(6)
α, deg	90	76.376(2)	118.107(2)
β, deg	96.775(2)	86.452(2)	103.647(2)
γ, deg	90	85.738(2)	103.659(2)
V, Å ³	7945.2(11)	3753.6(4)	4294.5(3)
Z	4	2	2
cryst syst	Monoclinic	Triclinic	Triclinic
space group	P 1 21/c 1	P -1	P -1
d _{calcd} , g/cm ³	1.399	1.501	1.495
θ range, deg	2.244 to 29.127	2.312 to 30.552	2.887 to 79.265
μ, mm ⁻¹	0.847	0.929	6.197
abs cor	Semi-empirical from equivalents	Semi-empirical from equivalents	Semi-empirical from equivalents
GOF ^c	1.043	1.021	1.017
R1, ^a wR2 ^b (I > 2σ(I))	0.0872, 0.2200	0.0940, 0.2788	0.0658, 0.1569

^a $R1 = \sum ||F_o| - |F_c|| / \sum |F_o|$ ^b $wR2 = \{ \sum [w(F_o^2 - F_c^2)^2] / \sum [w(F_o^2)^2] \}^{1/2}$ ^c $GOF = S = \{ \sum [w(F_o^2 - F_c^2)^2] / (n-p) \}^{1/2}$

REFERENCES

- 1.(a) Holm, R. H.; Kennepohl, P.; Solomon, E. I., *Chemical Reviews* **1996**, *96*, 2239-2314; (b) Ragsdale, S. W., *Chemical Reviews* **2006**, *106*, 3317-3337; (c) Fontecilla-Camps, J. C.; Amara, P.; Cavazza, C.; Nicolet, Y.; Volbeda, A., *Nature* **2009**, *460*, 814-822; (d) Can, M.; Armstrong, F. A.; Ragsdale, S. W., *Chemical Reviews* **2014**, *114*, 4149-4174; (e) Hoffman, B. M.; Lukoyanov, D.; Yang, Z. Y.; Dean, D. R.; Seefeldt, L. C., *Chemical Reviews* **2014**, *114*, 4041-4062; (f) Lubitz, W.; Ogata, H.; Rudiger, O.; Reijerse, E., *Chemical Reviews* **2014**, *114*, 4081-4148; (g) Solomon, E. I.; Heppner, D. E.; Johnston, E. M.; Ginsbach, J. W.; Cirera, J.; Qayyum, M.; Kieber-Emmons, M. T.; Kjaergaard, C. H.; Hadt, R. G.; Tian, L., *Chemical Reviews* **2014**, *114*, 3659-3853; (h) Yano, J.; Yachandra, V., *Chemical Reviews* **2014**, *114*, 4175-4205.
2. McEvoy, J. P.; Brudvig, G. W., *Chemical Reviews* **2006**, *106*, 4455-4483.
3. Solomon, E. I.; Sundaram, U. M.; Machonkin, T. E., *Chemical Reviews* **1996**, *96*, 2563-2606.
- 4.(a) Zhao, M.; Wang, H.-B.; Ji, L.-N.; Mao, Z.-W., *Chemical Society Reviews* **2013**, *42*, 8360-8375; (b) Warren, J. J.; Mayer, J. M., *Biochemistry* **2015**, *54*, 1863-1878.
- 5.(a) Meunier, B.; de Visser, S. P.; Shaik, S., *Chemical Reviews* **2004**, *104*, 3947-3980; (b) Denisov, I. G.; Makris, T. M.; Sligar, S. G.; Schlichting, I., *Chemical Reviews* **2005**, *105*, 2253-2278; (c) Ortiz de Montellano, P. R., *Chemical Reviews* **2010**, *110*, 932-948.
6. Rigsby, M. L.; Wasylenko, D. J.; Pegis, M. L.; Mayer, J. M., *Journal of the American Chemical Society* **2015**, *137*, 4296-4299.
- 7.(a) Taguchi, T.; Gupta, R.; Lassalle-Kaiser, B.; Boyce, D. W.; Yachandra, V. K.; Tolman, W. B.; Yano, J.; Hendrich, M. P.; Borovik, A. S., *Journal of the American Chemical Society* **2012**, *134*, 1996-1999; (b) Sano, Y.; Weitz, A. C.; Ziller, J. W.; Hendrich, M. P.; Borovik, A. S., *Inorganic Chemistry* **2013**, *52*, 10229-10231; (c) Cook, S. A.; Borovik, A. S., *Accounts of Chemical Research* **2015**, *48*, 2407-2414.
- 8.(a) MacBeth, C. E.; Golombek, A. P.; Young, V. G.; Yang, C.; Kuczera, K.; Hendrich, M. P.; Borovik, A. S., *Science* **2000**, *289*, 938-941; (b) Larsen, P. L.; Gupta, R.; Powell, D. R.; Borovik, A. S., *Journal of the American Chemical Society* **2004**, *126*, 6522-6523; (c) Lacy, D. C.; Gupta, R.; Stone, K. L.; Greaves, J.; Ziller, J. W.; Hendrich, M. P.; Borovik, A. S., *Journal of the American Chemical Society* **2010**, *132*, 12188-12190.
- 9.(a) Moore, C. M.; Szymczak, N. K., *Chemical Science* **2015**, *6*, 3373-3377; (b) Matson, E. M.; Park, Y. J.; Fout, A. R., *Journal of the American Chemical Society* **2014**, *136*, 17398-17401.
- 10.(a) Ng, G. K. Y.; Ziller, J. W.; Borovik, A. S., *Inorganic Chemistry* **2011**, *50*, 7922-7924; (b) Larsen, P. L.; Parolin, T. J.; Powell, D. R.; Hendrich, M. P.; Borovik, A. S., *Angewandte Chemie* **2003**, *115*, 89-93; (c) Zinn, P. J.; Powell, D. R.; Day, V. W.; Hendrich, M. P.; Sorrell, T. N.; Borovik, A. S., *Inorganic Chemistry* **2006**, *45*, 3484-3486; (d) Lee, J. H.; Park, J.; Lah, M. S.; Chin, J.; Hong, J.-I., *Organic Letters* **2007**, *9*, 3729-3731.
11. de Ruiter, G.; Thompson, N. B.; Lionetti, D.; Agapie, T., *Journal of the American Chemical Society* **2015**, *137*, 14094-14106.
12. Moss, T. A.; Addie, M. S.; Nowak, T.; Waring, M. J., *Synlett* **2012**, 285-289.
13. Tsui, E. Y.; Kanady, J. S.; Day, M. W.; Agapie, T., *Chemical Communications* **2011**, *47*, 4189-4191.
14. MacDonald, M. R.; Ziller, J. W.; Evans, W. J., *Inorganic Chemistry* **2011**, *50*, 4092-4106.
15. Davies, S. C.; Durrant, M. C.; Hughes, D. L.; Richards, R. L.; Sanders, J. R., *Journal of the Chemical Society, Dalton Transactions* **2000**, 4694-4701.
16. Sickerman, N. S.; Park, Y. J.; Ng, G. K. Y.; Bates, J. E.; Hilkert, M.; Ziller, J. W.; Furche, F.; Borovik, A. S., *Dalton Transactions* **2012**, *41*, 4358-4364.

- 17.(a) MacBeth, C. E.; Gupta, R.; Mitchell-Koch, K. R.; Young, V. G.; Lushington, G. H.; Thompson, W. H.; Hendrich, M. P.; Borovik, A. S., *Journal of the American Chemical Society* **2004**, *126*, 2556-2567; (b) Mukherjee, J.; Lucas, R. L.; Zart, M. K.; Powell, D. R.; Day, V. W.; Borovik, A. S., *Inorganic Chemistry* **2008**, *47*, 5780-5786.
- 18.Pangborn, A. B.; Giardello, M. A.; Grubbs, R. H.; Rosen, R. K.; Timmers, F. J., *Organometallics* **1996**, *15*, 1518-1520.
- 19.Fulmer, G. R.; Miller, A. J. M.; Sherden, N. H.; Gottlieb, H. E.; Nudelman, A.; Stoltz, B. M.; Bercaw, J. E.; Goldberg, K. I., *Organometallics* **2010**, *29*, 2176-2179.